Segmented spiral waves in a reaction-diffusion system

Vladimir K. Vanag* and Irving R. Epstein*

Department of Chemistry and Volen Center for Complex Systems, Brandeis University, Waltham, MA 02454

Edited by Gerhard Ertl, Max Planck Society for the Advancement of Science, Berlin, Germany, and approved October 16, 2003 (received for review July 30, 2003)

Pattern formation in reaction-diffusion systems is often invoked as a mechanism for biological morphogenesis. Patterns in chemical systems typically occur either as propagating waves or as stationary, spatially periodic, Turing structures. The spiral and concentric (target) waves found to date in spatially extended chemical or physical systems are smooth and continuous; only living systems, such as seashells, lichens, pine cones, or flowers, have been shown to demonstrate segmentation of these patterns. Here, we report observations of segmented spiral and target waves in the Belousov–Zhabotinsky reaction dispersed in water nanodroplets of a water-in-oil microemulsion. These highly ordered chemical patterns, consisting of short wave segments regularly separated by gaps, form a link between Turing and trigger wave patterns and narrow the disparity between chemistry and biology. They exhibit aspects of such fundamental biological behavior as self-replication of structural elements and preservation of morphology during evolutionary development from a simpler precursor to a more complex structure.

The visually striking spiral concentration waves found in a number of reaction-diffusion systems have fascinated scientists since their discovery (1) in the Belousov–Zhabotinsky (BZ) system more than three decades ago. Subsequent observations of spiral patterns in such diverse systems as aggregating slime molds (2), developing oocytes (3), cardiac muscle (4, 5), spreading depression in chicken retina (6), Rayleigh–Bénard convection (7), catalytic crystal surfaces (8), and galaxies (9) have served to emphasize the importance of understanding this phenomenon and the related concentric ring (target) patterns (10). Further study of spiral waves has revealed the existence of more complex phenomena, including multiarmed (11), super- (12), ripple- (13), zigzag- (14), and inwardly propagating (anti-) spirals (15). The BZ reaction, the oxidation of malonic acid (MA) by bromate, catalyzed by metallo-complexes in acidic aqueous solution, remains the prototype system, in which all of these spiral variants have been found.

If reagents of the BZ reaction are dispersed in a water-in-oil aerosol sodium bis(2-ethylhexyl) sulfosuccinate (AOT) microemulsion (ME) (BZ-AOT system), new types of patterns, particularly stationary Turing patterns (16) and dash waves (17), are found. The BZ-AOT system exhibits an extremely rich variety of dynamical concentration patterns, which can be stable only far from equilibrium. An AOT-ME consists of nanometer-sized water droplets dispersed in a continuous oil (octane) phase. Each droplet is surrounded by a surfactant, AOT, monolayer. The polar BZ reagents are dissolved in the aqueous phase, i.e., in the water droplets. At the high concentrations of sulfuric acid and bromate used in the reaction, a freshly prepared ME consists of two pools of droplets with different radii, ≈2–3 and 10–20 nm (17). Since chemical reactivity in nano-droplets depends on droplet radius, the two pools of droplets constitute two slightly different chemical subsystems coupled through the oil phase by oil-soluble intermediates of the reaction (Br_2 or $BrO_2^{\cdot}$) and/or by droplet collision/fusion/fission. In a narrow range of reagent concentrations, the BZ-AOT system has two steady states, one stable and spatially homogeneous but excitable, in which a local superthreshold perturbation generates trigger waves, the other a spatially inhomogeneous pseudo-Turing unstable steady state with a characteristic Turing wavelength, which is driven to a different stable state, steady or oscillatory, by an infinitesimal perturbation. A smooth plane trigger wave propagating in such a medium can break into dashes and gaps (17). In this article, we report the occurrence of stable segmented spirals in the bathoferroin-catalyzed BZ-AOT system.

Materials and Methods

Bathophenanthroline (BP, 4,7-diphenyl-1,10-phenanthroloine, Aldrich), which is insoluble in both water and pure octane, is first dissolved in a 1.5 M solution of AOT in octane (12.3 mM). Large crystals of BP require 1–2 days to dissolve, but powder samples take only ≈1 h. Water and 1 M $NaBrO_3$ are added in such a way that the resulting ME has $\omega \equiv [H_2O]/[AOT] \cong 15$, volume droplet fraction (water + surfactant) $\varphi_d \cong 0.7$, and the desired concentration of $NaBrO_3$. The ratio ω roughly determines the average radius of water nano-droplets as $R_w \cong 0.17\ \omega$ (nm). Then, a small droplet of 0.25 M $FeSO_4$ is added so that $[BP]/[Fe^{2+}] = 3$ and $\varphi_d = 0.71$ in the final ME-1. ME-2 also has $\omega = 15$, $\varphi_d = 0.71$ and contains the desired concentrations of MA and H_2SO_4. The final reactive ME is obtained by mixing ME-1 with ME-2 (1:1) and enough pure octane to give the desired φ_d at $\omega = 15$. The initial concentrations (M) in the aqueous pseudophase are $[c]_w = [c]_S$: $[MA]_w = 0.3$, $[H_2SO_4]_w = 0.2$, $[NaBrO_3]_w = 0.18$, $[\text{bathoferroin}]_w = 0.0049$, where the subscript w refers to concentrations in the aqueous pseudophase. The bulk (total) concentration, $[c]_b$, is determined as $[c]_b = \varphi_w[c]_w$ and φ_w is the volume fraction of the aqueous pseudophase, $\varphi_w \cong \varphi_d/(1 + 21.7/\omega)$.

A small droplet (≈0.1 ml) of reactive ME is sandwiched between two flat windows separated by an annular Teflon gasket (Zefluor membrane) of thickness 80 μm, inner diameter 25 mm, and outer diameter 47 mm. This arrangement constitutes our reactor. The edges of the reactor are sealed with Teflon tape, and then the two windows are pressed together in a window holder. Patterns are observed at 23.5°C through a microscope or a tele (long focus) objective both equipped with a digital charge-coupled device camera connected to a computer. The reactor is illuminated through a 532-nm interference filter. The percolation threshold, as measured by the electrical conductivity, σ, occurs at about $\varphi_d = 0.5$–0.6. As we increase the droplet fraction through this value, σ jumps from ≈1 to ≈100 μS, indicating the formation of water channels that span the medium. For segmented spirals, $\sigma < 1\ \mu$S. The droplet radii are measured by dynamic light scattering (DynaPro, Protein Solutions, High Wycombe, U.K.).

This paper was submitted directly (Track II) to the PNAS office.

Abbreviations: BZ, Belousov–Zhabotinsky; AOT, aerosol sodium bis(2-ethylhexyl) sulfosuccinate; ME, microemulsion; MA, malonic acid.

*To whom correspondence should be addressed. E-mail: vanag@brandeis.edu or epstein@brandeis.edu.

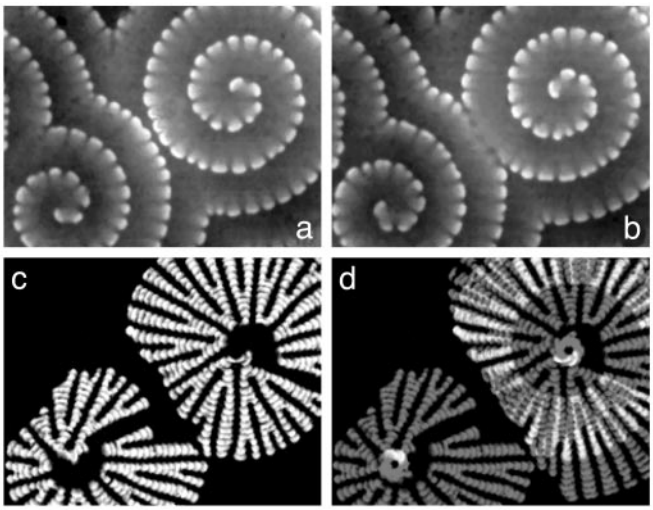

Fig. 1. Segmented spirals in a BZ-AOT ME. Stroboscopic composites (*c* and *d*) show trajectories built from spiral segments (*a* and *b*). (*c*) Superposition of snapshots taken every 50 s of segments of spiral turns initially closest to the cores. (*d*) Summation of c and trajectories of segments of the second turn of the spiral at the upper right; the two ''eyes'' are derived from the tip segments only. White corresponds to higher concentration of bathoferriin in *a* and *b* and marks overlapping trajectories in *c* and *d*. $\varphi_d = 0.36$. Frame size (mm^2), 3.72 by 4.82. Time between *a* and *b* is 66 s.

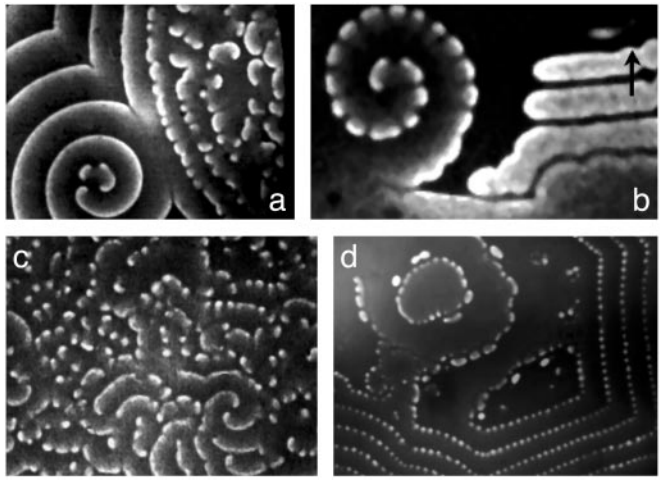

Fig. 2. The birth (*a* and *b*) and death (*c* and *d*) of segmented spirals. (*a*) Transformation of an ordinary spiral into a segmented one. (*b*) A small segmented spiral on an oscillatory background; the arrow marks the direction of stripe-like propagation of the front. (*c*) Chaotic dash waves after destruction of the spiral core. (*d*) Regular dash waves with bubbles in the reactor center, $[c]_w = [c]_S$. $\varphi_d = 0.36$ (*a* and *d*) and 0.47 (*b* and *c*). Size (mm^2) = 3.8 by 5.0 (*a*), 1.93 by 2.86 (*b*), 3.7 by 4.9 (*c*), and 8.85 by 11.8 (*d*).

Results

Segmented Spirals. A typical pair of segmented spirals is shown in Fig. 1 *a* and *b*. These spirals are sustained by the continuous production of new segments (see Movie 1, which is published as supporting information on the PNAS web site). The tip of the spiral is a single continuously rotating segment (a short trigger wave), which grows, reaches a critical length (≈0.21–0.24 mm) and splits, emitting a new segment. All segments, although not the intervening gaps, grow as the wave propagates away from the spiral core. When a segment attains the critical length, it splits, thereby maintaining the average length of dashes and gaps approximately constant (λ_T = gap + segment ≅ 0.28–0.3 mm, see trajectories of segments in Fig. 1 *c* and *d*). The core of the spiral (black ''eyes'' in Fig. 1*d*) is ≈0.12 mm in diameter, comparable to the gap length. The splitting of segments resembles the division of living cells or of spots in the ferrocyanide-iodate-sulfite reaction (18) or Turing spots (blobs) in the chlorine dioxide-iodine-MA reaction (19). As in living cells, younger segments, which are closer to the spiral core, grow faster and divide more often than older segments, which are far from the core. Quantitatively, the frequency of splitting, *f*, depends on the distance *r* from the center as $f = (v_S/r)[1.65 + \log_2(r/\lambda_T)]$, where v_S is the transverse velocity of a segment. Far from the core, in the outermost regions of the spiral, the segments are nearly straight ($r \cong \infty$), like planar dash waves (17), the segments of which maintain constant length during propagation (Fig. 2*d*).

The segments of one spiral cannot penetrate through the gaps of another; when waves of two neighboring segmented spirals collide, they annihilate. However, unlike annihilation of ordinary waves, a faint dark line composed of gaps persists for some time in place of annihilated segmented waves (Fig. 1*b*). Radial dark lines half a spiral pitch in length are also seen behind each gap (Figs. 1 *a* and *b* and 2*b*).

To understand better the conditions necessary for segmented spirals, it is useful to follow their emergence. Segmented spirals always arise from preexisting ordinary spirals. The latter emerge spontaneously almost immediately after we sandwich a droplet of reactive ME between two windows to form our batch reactor. After an induction period T_{ind} (T_{ind} = 10–40 min; the larger the volume fraction of droplets φ_d, the shorter the induction period) the conditions necessary for segmentation of waves are satisfied first near the reactor border (the edge of the Teflon gasket), where dash-waves appear and move toward the center of the reactor. At the beginning of segmentation, the dash waves propagate faster than the zone of segmentation, and dash waves are transformed into ordinary waves at the border of this region. For a while, the ordinary spirals and dash waves coexist. Later, when a set of dash waves approaches an ordinary spiral, the latter begins to develop breaks and eventually transforms into a segmented spiral (see Movie 2, which is published as supporting information on the PNAS web site).

The process of spiral segmentation always begins at the spiral center (Fig. 2*a*), apparently because of the radial dependence of the wave velocity $v(r)$. According to the eikonal equation (20) and its modification for our case of a rapidly diffusing inhibitor (21), $v(r) = c_0 - D_{act}/r$, where c_0 depends on the ratio D_{inh}/D_{act} (>1) and to a much weaker extent on *r* (c_0 coincides with the velocity of a plane wave if $D_{inh} = D_{act}$) and D_{act} and D_{inh} are the diffusion coefficients of the activator and inhibitor species, respectively. The wave velocity is therefore smallest at the spiral core. The low velocity, v_S, and rotation frequency, ω_S, of segmented spirals appear to be necessary for their emergence and stability; v_S and ω_S are significantly smaller than the corresponding quantities for the ordinary spiral trigger waves (v_o, ω_o), from which they originate [v_S = 1.5–1.8 μm/s and ω_S = 0.019–0.022 s^{-1}, while v_o = 3.4–4.5 μm/s and ω_o = 0.044–0.050 s^{-1} at φ_d = 0.36–0.47 and $[c]_w = [c]_S$ (see *Materials and Methods*)]. Segmentation results, first, in the emergence of curved fragments of smooth wave, whose presence slows down the wave caused by the eikonal equation. Wave deceleration, in turn, promotes further segmentation, since the pseudo-Turing instability requires time to develop. In a sense, then, segmentation is a self-accelerating process.

Segmented spirals are found both when a reactive ME exhibits (conditions of Fig. 2*b*), and also when it does not display (conditions of Fig. 1 *a* and *b*), bulk oscillations in a continuously stirred tank reactor. Thus, the emergence of segmented spirals is independent of the occurrence of a Hopf bifurcation.

The destruction of segmented spirals also confirms that these

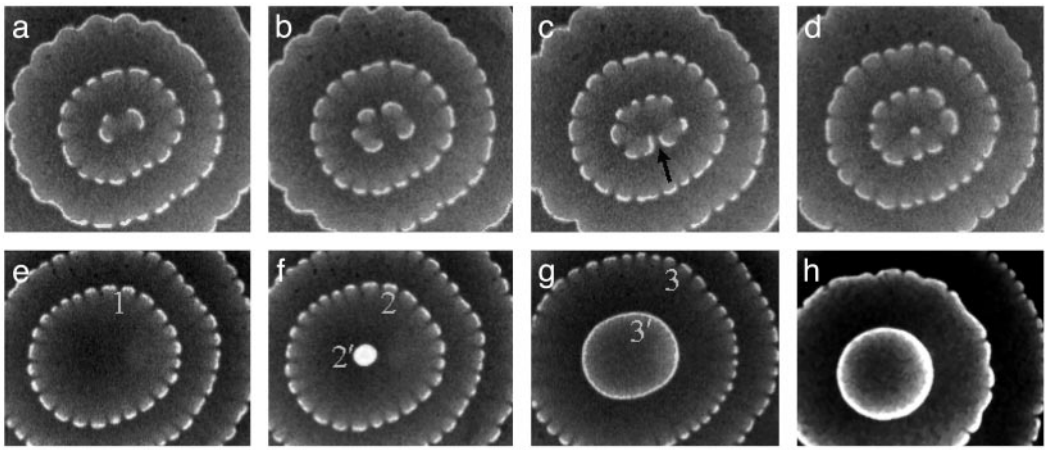

Fig. 3. Segmented target patterns. $[c]_w = [c]_S$, $\varphi_d = 0.36$. Size (mm^2) = 2.23 by 2.42 (*a–d*), 3.8 by 4.8 (*e–g*), and 3.8 by 5.0 (*h*). Time elapsed between snapshots in *a–d*: 59, 52, and 50 s; between first three snapshots of *e–h*: 24 and 218 s. Δt between *g* and *h* is ≈1 h (the reactor was shifted during this time). Numbers 1, 2, and 3 in *e–g* mark the same segmented wave, and 2′ and 3′ mark the same smooth wave.

waves cannot emerge spontaneously, but require a smooth spiral as a precursor pattern. If we annihilate a spiral core with a small gas bubble, the spiral is irreversibly transformed into a chaotic pattern. Chaos generated in this fashion (Fig. 2*c*) appears to persist indefinitely (it lasted for several hours in our batch experiments). Each segment wave moves in an arbitrary direction, grows, splits into two, and collides and annihilates with other segments.

Related Patterns. If, instead of a spiral, a target pattern is present initially, a segmented target pattern ("flower") emerges (Fig. 3 *a-d*), which, however, is not stable. A small central segment, as shown in Fig. 3*d*, results from the "imperfect" annihilation, indicated in Fig. 3*c* by an arrow, of two colliding segments, one of which is slightly longer than the other. The sequence in Fig. 3 *a-d* is typically repeated several times, ultimately leading to the disappearance of the central wave segment (perfect annihilation, Fig. 3*e*). After a delay, a new circular wave emerges and spreads rapidly without breaks (Fig. 3 *f* and *g*). During the first 10–20 s, this smooth wave travels at 80–90 μm/s. As it approaches the nearest segmented wave, it gradually decelerates to 2 μm/s and then begins to break into segments, like the middle wave in Fig. 3*h*. This phenomenon supports the contention that a low wave velocity is necessary for segmented circular and spiral waves. Similar behavior was noted in propagating cellular fronts (22).

Varying φ_d and the reactant concentrations by <10% around $\varphi_d = 0.36$ and $[c]_S$, we find "bubbles," i.e., small concentric waves, the centers of which, unlike segments, are stationary. In many experiments, segmented spirals evolved into bubbles over several hours (center of Fig. 2*d*). At slightly larger deviations (±20%) from $\varphi_d = 0.36$ or $[c]_S$ (e.g., $[MA]_w = 0.40$ M or 0.25 M at $\varphi_d = 0.28$ or 0.47; or $[H_2SO_4]_w = 0.15$ M at $\varphi_d = 0.36$), we find mainly standing waves. Circular standing waves are intermediate patterns between propagating fronts of stripes (Fig. 2*b*) and spot-like standing waves. Propagating stripe fronts are, in turn, an intermediate dynamic behavior between propagating fronts of bubbles and standing waves. A typical path through the parameter space yields the following sequence of patterns: smooth trigger waves (ordinary spirals) → ripple waves → dash waves (segmented spirals) → front of bubbles → chaotic bubbles/front of stripes → standing waves (circular and spot-like).

Discussion and Conclusion

Different patterns (dash waves or segmented spirals, bubbles, propagating stripes) can coexist in different parts of the reactor (Fig. 2 *b* and *d*), a phenomenon that may result from multistability among the various pattern types. This hypothesis is supported by the fact that fronts of bubbles or stripes often occur between two neighboring regions of segmented spirals or dash waves. After two waves collide and annihilate, the resulting quiescent area stays intact long enough for spontaneous bubble formation to occur before the arrival of the nearest dash or segmented waves, which propagate slowly.

Segmented spirals have multiple breaks, but only the segment closest to the spiral tip curls and rotates. In contrast, the ends of ordinary trigger waves, in accordance with the eikonal equation, begin to curl as soon as the wave is broken, leading to the emergence of new spirals. One appealing explanation for this difference is that the convex segments do, in fact, start to curl, but because their tips annihilate with those of neighboring curled segments, they fail to generate new spirals and simply propagate ahead. The gap length should be a determining factor in this process, since large gaps would allow segments to curl, as is seen in chaotic dash waves (Fig. 2*c*), which have larger distances between their segments.

The polydisperse distribution of segment lengths, which is inevitable for segments that constantly grow and split, might, in principle, constitute a source of instability for segmented spirals. Applying the eikonal equation to individual segments would imply that longer segments, which have smaller curvature, propagate faster than shorter segments, leading to transverse breaking of spirals. We do not, however, observe such a phenomenon at $\varphi_d = 0.36$ and $[c]_S$; segmented spirals are stable.

A mechanism proposed for the emergence of dash waves (17), which should apply to segmented spirals as well, suggests that segmented spirals are propagating 1D Turing structures in a system possessing several steady states, one of which is excitable, whereas another is pseudo-Turing unstable. The properties of such a medium imply that the pseudo-Turing instability occurs only in regions that contain waves, where the excitability of the system enables it to switch to the Turing-unstable steady state. This type of spatial "inhomogeneity" or "bistability" differentiates segmented spirals from other types of tangential (lateral) instabilities of fronts found, for example, in reaction-diffusion systems with cubic autocatalysis (23) or in the case of spreading 2D Turing patterns† (19).

†Note that figure 6 in ref. 19 resembles our Fig. 1 *c* or *d*, except that our patterns are traces of spiral segments, whereas the figure in ref. 19 represents actual Turing patterns ("chemical flowers").

The segmented spirals found here are complex dynamical structures with several levels of organization, characterized, for example by the wavelength λ between successive spiral turns and the Turing wavelength λ_T between segments. The appearance and complexity of segmented spirals are suggestive of phenomena in living systems. The trajectories of the segmented spirals in Fig. 1 *c* and *d* are reminiscent of corals or the streaming patterns of the slime mold *Dictyostelium discoideum* (24). Segmented spirals may provide a better model for these streaming patterns than the ordinary spiral waves of cyclic adenosine monophosphate that are often invoked (25). Phyllotaxis, the arrangement of leaves in many plants (26), constitutes another striking example of segmented spirals in nature.

We thank Milos Dolnik, Lingfa Yang, and Anatol Zhabotinsky for helpful discussions. This work was supported by the Chemistry Division of the National Science Foundation.

1. Winfree, A. T. (1972) *Science* **175,** 634–636.
2. Tomchik, K. J. & Devreotes, P. N. (1981) *Science* **212,** 443–446.
3. Lechleiter, J., Girard, S., Peralta, E. & Clapham, D. (1991) *Science* **252,** 123–126.
4. Davidenko, J. M., Pertsov, A. V., Salomonsz, R., Baxter, W. & Jalife, J. (1992) *Nature* **355,** 349–351.
5. Winfree, A. T. (1994) *Science* **266,** 1003–1006.
6. Gorelova, N. A. & Bures, J. (1983) *J. Neurobiol.* **14,** 353–363.
7. Ecke, R. E., Hu, Y., Mainieri, R. & Ahlers, G. (1995) *Science* **269,** 1704–1707.
8. Ertl, G. (1991) *Science* **254,** 1750–1755.
9. Schulman, L. S. & Seiden, P. E. (1986) *Science* **223,** 425–431.
10. Zaikin, A. N. & Zhabotinsky, A. M. (1970) *Nature* **225,** 535–537.
11. Agladze, K. & Krinsky, V. I. (1982) *Nature* **296,** 424–426.
12. Perez-Munuzuri, V., Aliev, R., Vasiev, B., Perez-Villar, V. & Krinsky, V. I. (1991) *Nature* **353,** 740–742.
13. Markus, M., Kloss, G. & Kusch, I. (1994) *Nature* **371,** 402–404.
14. Astrov, Yu. A., Muller, I., Ammelt, E. & Purwins, H.-G. (1998) *Phys. Rev. Lett.* **80,** 5341–5344.
15. Vanag, V. K. & Epstein, I. R. (2001) *Science* **294,** 835–837.
16. Vanag, V. K. & Epstein, I. R. (2001) *Phys. Rev. Lett.* **87,** 228301.
17. Vanag, V. K. & Epstein, I. R. (2003) *Phys. Rev. Lett.* **90,** 098301.
18. Lee, K. J., McCormick, W. D., Pearson, J. E. & Swinney, H. L. (1994) *Nature* **369,** 215–218.
19. Davies, P. W., Blanchedeau, P., Dulos, E. & De Kepper, P. (1998) *J. Phys. Chem. A* **102,** 8236–8244.
20. Keener, J. P. & Tyson, J. J. (1986) *Physica D* **21,** 307–324.
21. Zykov, V. S., Mikhailov, A. S. & Muller, S. C. (1998) *Phys. Rev. Lett.* **81,** 2811–2814.
22. Fuentes, M., Kuperman, M. N. & De Kepper, P. (2001) *J. Phys. Chem. A* **105,** 6769–6774.
23. Horvath, D. & Showalter, K. (1995) *J. Chem. Phys.* **102,** 2471–2478.
24. Ben-Jacob, E., Cohen, I. & Levine, H. (2000) *Adv. Phys.* **49,** 395–554.
25. Vasiev, B. N., Hogeweg, P. & Panfilov, A. V. (1994) *Phys. Rev. Lett.* **73,** 3173–3176.
26. Saunders, P. T., ed. (1992) *Morphogenesis* (Elsevier, Amsterdam).